EBioMedicine 21 (2017) 218–227

Contents lists available at ScienceDirect

EBioMedicine

journal homepage: www.ebiomedicine.com

Research Paper

Reduced TDP-43 Expression Improves Neuronal Activities in a *Drosophila* Model of Perry Syndrome

Yuka Hosaka [a], Tsuyoshi Inoshita [b], Kahori Shiba-Fukushima [b], Changxu Cui [c], Taku Arano [d], Yuzuru Imai [a,b,*], Nobutaka Hattori [a,b,c,*]

[a] Department of Neurology, Juntendo University, Graduate School of Medicine, Tokyo 113-8421, Japan
[b] Department of Treatment and Research in Multiple Sclerosis and Neuro-intractable Disease, Juntendo University, Graduate School of Medicine, Tokyo 113-8421, Japan
[c] Department of Research for Parkinson's Disease, Juntendo University, Graduate School of Medicine, Tokyo 113-8421, Japan
[d] Center for Genomic and Regenerative Medicine, Juntendo University, Graduate School of Medicine, Tokyo 113-8421, Japan

ARTICLE INFO

Article history:
Received 15 February 2017
Received in revised form 29 May 2017
Accepted 1 June 2017
Available online 8 June 2017

Keywords:
Dynactin
TDP-43
Axonal transport
Dopamine
Parkinsonian syndrome
Neurodegeneration

ABSTRACT

Parkinsonian Perry syndrome, involving mutations in the dynein motor component dynactin or p150^{Glued}, is characterized by TDP-43 pathology in affected brain regions, including the substantia nigra. However, the molecular relationship between p150^{Glued} and TDP-43 is largely unknown. Here, we report that a reduction in TDP-43 protein levels alleviates the synaptic defects of neurons expressing the Perry mutant p150^{G50R} in *Drosophila*. Dopaminergic expression of p150^{G50R}, which decreases dopamine release, disrupts motor ability and reduces the lifespan of *Drosophila*. p150^{G50R} expression also causes aggregation of dense core vesicles (DCVs), which contain monoamines and neuropeptides, and disrupts the axonal flow of DCVs, thus decreasing synaptic strength. The above phenotypes associated with Perry syndrome are improved by the removal of a copy of *Drosophila* TDP-43 TBPH, thus suggesting that the stagnation of axonal transport by dynactin mutations promotes TDP-43 aggregation and interferes with the dynamics of DCVs and synaptic activities.

1. Introduction

Perry syndrome (PS) is an autosomal dominant disorder characterized by parkinsonism with depression, sleep disturbance, weight loss, and central hypoventilation (Perry et al., 1975; Wider and Wszolek, 2008; Farrer et al., 2009). Genome-wide linkage analysis has identified disease-segregating missense mutations located in the *dynactin* (*DCTN1*) gene (Farrer et al., 2009). The gene product of *dynactin*, p150^{Glued}, forms a complex with dynein, the microtubule-dependent retrograde motor. Disease-associated missense mutations (G71R, G71E, G71A, T72P, Q74P) are located in the cytoskeleton-associated protein Gly-rich (CAP-Gly) domain of p150^{Glued}, which has been implicated in binding to microtubules recruiting dynein (Farrer et al., 2009; Ayloo et al., 2014; Tacik et al., 2014) and stabilizing the plus-end of microtubules (Lazarus et al., 2013). A glycine to serine substitution at residue 59 (G59S), which causes distal hereditary motor neuropathy 7B (HMN7B) (Puls et al., 2003), appears to affect the structure of the CAP-Gly domain and produces severe synaptic phenotypes, including p150^{Glued} aggregation, dynein accumulation at nerve terminals and disruption of axonal transport (Lloyd et al., 2012; Moughamian and Holzbaur, 2012). Mutations associated with PS show milder synaptic phenotypes but cause impaired retrograde flux (Lloyd et al., 2012; Moughamian and Holzbaur, 2012).

The TAR DNA-binding protein of 43 kDa (TDP-43) is a highly conserved heterogeneous ribonucleoprotein (hnRNP) involved in the transcription, splicing, stabilization and transport of specific mRNAs (Volkening et al., 2009; Fiesel et al., 2010; Polymenidou et al., 2011; Ling et al., 2015). TDP-43 has been identified as the key component of intracellular ubiquitin-positive inclusions observed in affected brain areas of patients with amyotrophic lateral sclerosis (ALS), frontotemporal lobar degeneration (FTLD) and Alzheimer's disease (Arai et al., 2006; Neumann et al., 2006; Josephs et al., 2015; Tan et al., 2015; McAleese et al., 2017). A pathological feature of PS is the accumulation of TDP-43 in affected areas (Farrer et al., 2009; Wider et al., 2009). Increased TDP-43 is toxic to neurons (Li et al., 2010; Swarup et al., 2011), possibly because of its proneness to aggregation and conversion to an abnormal protein structure similar to that of prion and α-Synuclein (Nonaka et al., 2013). On the other hand, TDP-43 is indispensable to mouse development (Chiang et al., 2010; Sephton et al., 2010) and *Drosophila* survival (Feiguin et al., 2009; Diaper et al., 2013b; Vanden Broeck et al., 2013), thus suggesting that the control of appropriate protein levels is critical for TDP-43 function.

* Corresponding authors at: Department of Neurology, Juntendo University, Graduate School of Medicine, Tokyo 113-8421, Japan.
E-mail addresses: yzimai@juntendo.ac.jp (Y. Imai), nhattori@juntendo.ac.jp (N. Hattori).

http://dx.doi.org/10.1016/j.ebiom.2017.06.002

The molecular relationship between p150^{Glued} and TDP-43 is largely unknown. To determine whether TDP-43 contributes to PS phenotypes, we manipulated TDP-43 protein levels in a *Drosophila* PS model and found that reduced TDP-43 improved defects in axonal transport and the synaptic activity of central dopaminergic neurons, as well as motor neurons, caused by the neuron-specific expression of a PS-associated p150^{Glued} mutation.

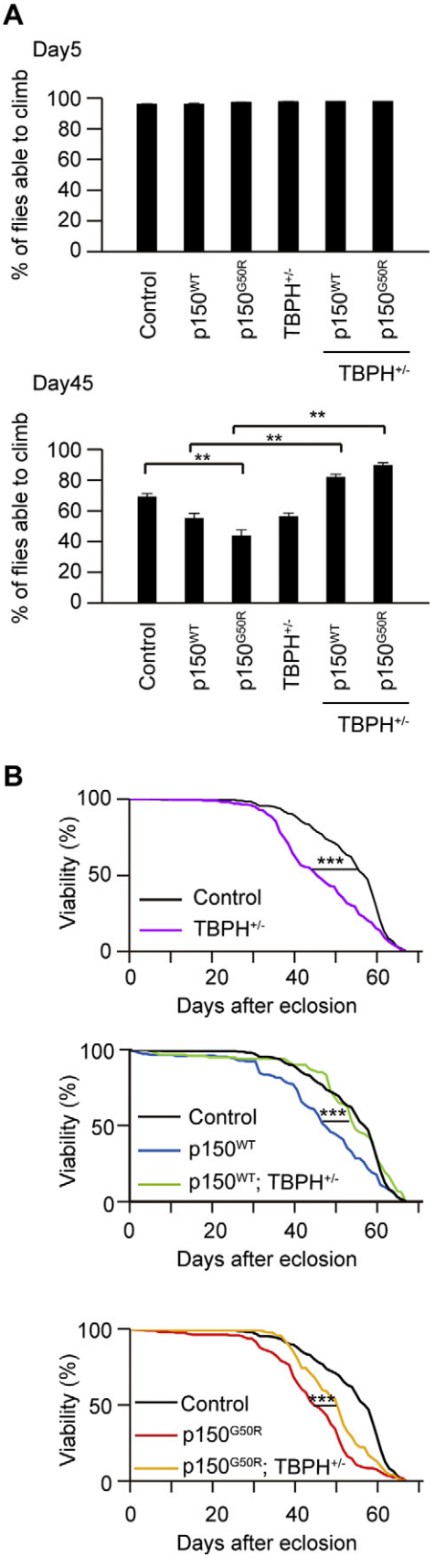

2. Materials and Methods

2.1. Drosophila Strains

Fly culture and crosses were performed on standard fly food containing yeast, cornmeal, and molasses. Flies were raised at 25 °C. All other fly stocks and *GAL4* lines used in this study were obtained from the Bloomington *Drosophila* Stock Center and Kyoto Stock Center and have previously been described: *UAS-p150^{WT}-HA* and *UAS-p150^{G50R}-HA* (Lloyd et al., 2012); *TBPH$^{\Delta 23}$* (Feiguin et al., 2009); *UAS-GFP-TBPH^{WT}*, *UAS-RFP-TBPH^{WT}* and *UAS-RFP-TBPH^{A315T}* (Estes et al., 2011); and *UAS-VMAT-phluorin* (Wu et al., 2013). Stocks were backcrossed to the *w^{1118}* wild-type background for six generations, and *w^{1118}* was used as a wild-type allele.

2.2. Survival Assay and Climbing Assay

For lifespan studies, approximately 20 adult flies per vial were maintained at 25 °C, transferred to fresh fly food, and scored for survival every 4 days. To control for isogeny, fly lines were backcrossed to the *w^{1118}* background for six generations. A climbing assay was performed as previously described (Shiba-Fukushima et al., 2014). For spontaneous locomotor behavior, male flies were preconditioned at 25 °C under a 12-h light: dark cycle for 3 days and were then recorded for another 3 days using a *Drosophila* activity monitoring (DAM) system (TriKinetics), which monitors the activity of individual flies (16 to 32 flies per experiment) in polycarbonate tubes (length, 65 mm; inside diameter, 3 mm).

2.3. Whole-mount Immunostaining and Transmission Electron Microscopy (TEM) Analysis

The antibodies used in immunocytochemistry were anti-Bruchpilot (1:10, Developmental Studies Hybridoma Bank (DSHB), nc82, RRID:AB_2314867), anti-GluRIIA (1:10, DSHB, 8B4D2, RRID:AB_528269), anti-Dlg (1:250, DSHB, 4F3, RRID:AB_528203), anti-GFP (1:500, Thermo Fisher Scientific, A6455, RRID:AB_221570), anti-RFP (1:100, Abcam, ab62341, RRID:AB_945213), and Alexa Fluor594- (1:200) or DyLight649- (1:500) conjugated anti-horseradish peroxidase (HRP) (Jackson ImmunoResearch, 123-585-021, RRID:AB_2338966 and 123-495-021, discontinued). The visualizations of synapse boutons, mitoGFP and active zones (AZs) in larval motor neurons were analyzed by whole-mount immunostaining as previously described (Lee et al., 2010). For image processing of synapse boutons, thirty *Z*-stack images were taken at 0.15- to 0.30-μm intervals and were reconstituted using ImageJ. TEM images were obtained using an electron microscope (Hitachi, HT7700) at the Laboratory of Ultrastructural Research of Juntendo University.

Fig. 1. Reducing endogenous TBPH rescues motor impairment caused by dopaminergic expression of p150^{G50R}. (A) Climbing assay at 5 and 45 days old. $n = 15$ trials in 20 flies per genotype, $^{**}p < 0.01$ by Tukey-Kramer test. (B) Lifespan at 25 °C. $^{***}p < 0.001$ by log-rank test. See also Fig. S1. Genotypes in (A, B) and sample size in (B) are: *TH-Gal4/+* (Control, $n = 298$), *UAS-p150^{WT}-HA/+; TH-Gal4/+* (p150^{WT}, $n = 188$), *UAS-p150^{G50R}-HA/+; TH-Gal4/+* (p150^{G50R}, $n = 251$), *TBPH$^{\Delta 23}$/+; TH-Gal4/+* (TBPH$^{+/-}$, $n = 202$), *TBPH$^{\Delta 23}$/+; UAS-p150^{WT}-HA; TH-Gal4/+* (p150^{WT}; TBPH$^{+/-}$, $n = 149$), *TBPH$^{\Delta 23}$/+; UAS-p150^{G50R}-HA; TH-Gal4/+* (p150^{G50R}; TBPH$^{+/-}$, $n = 168$).

2.4. Immunoprecipitation and Western Blot Analysis

To analyze the binding between TBPH and p150^{Glued}, eight 3rd-instar larvae (w^{1118}) from which the digestive organs had been removed were lysed with 200 μl lysis buffer (Tris-HCl, pH 7.6, 150 mM NaCl, 1% NP-40, 5% glycerol, 1 mM EDTA, 1 mM DTT) containing Complete protease inhibitor cocktail (Sigma-Aldrich) with a motor-driven pestle. Supernatant obtained after centrifugation at 16,000 ×*g* for 10 min was subjected to immunoprecipitation with anti-p150^{Glued} conjugated with TrueBlot Magnetic Beads (Rockland Immunochemicals Inc., RRID:AB_2610703) and was incubated at 4 °C overnight. The beads washed three times with the lysis buffer were analyzed by subsequent western blotting. For western blotting to determine protein levels, larvae from which the digestive organs had been removed were homogenized in 10 μl of RIPA buffer (20 mM Tris-HCl, pH 7.4, 150 mM NaCl, 2 mM EDTA 1% NP-40, 1% deoxycholate, 0.1% SDS) containing Complete protease inhibitor cocktail per sample using a motor-driven pestle. After centrifugation at 16,000 ×*g* for 10 min, the supernatants dissolved in SDS sample buffer were subjected to western blotting. The antibodies used in western blotting were anti-GluRIIA (1:50, DSHB, 8B4D2), anti-Dlg (1:1000, DSHB, 4F3), anti-Dynein (1:50, DSHB, 2C11-2, RRID:AB_2091523), anti-β-Tubulin (1:50, DSHB, E7, RRID:AB_528499), anti-HA (1:1000, Sigma-Aldrich, 3F10, RRID:AB_390919), anti-TBPH (1:1000) and anti-p150^{Glued} (1:1000, C). Anti-TBPH and anti-p150^{Glued} (N and C) antibodies were kind gifts from Drs. F. Hirth and V.I. Gelfand, respectively (Siller et al., 2005; Diaper et al., 2013a).

2.5. Dopamine Measurement

Five adult male fly heads were dissected and homogenized in 50 μl of 0.1 M perchloric acid by using a motor-driven pestle around 1 p.m. Dopamine levels in *Drosophila* brain extracts were determined by HPLC coupled to electrochemical detection using a mobile phase containing 50 mM citric acid, 50 mM sodium dihydrogen phosphate, pH 2.5, 0.1 mM EDTA, 4.4 mM 1-heptanesulfonic acid, 2.2% (vol/vol) acetonitrile, and 5.3% (vol/vol) methanol.

2.6. Live Imaging of Axonal Transport

Living 3rd-instar larvae were dissected in HL-3 saline (5 mM HEPES, pH 7.2, 70 mM NaCl, 5 mM KCl, 20 mM $MgCl_2$, 10 mM $NaHCO_3$, 115 mM sucrose, 5 mM trehalose, and 2 mM $CaCl_2$). Time-lapsed images (0.1 s interval during 36 s) were captured using a laser-scanning microscope system (TCS-SP5, Leica). Imaging data were processed with ImageJ software.

2.7. Electrophysiology

Third-instar larvae were dissected in HL-3, and mEJPs from NMJs were recorded using an electrophysiological setup equipped with an Eclipse FN1 microscope (Nikon), a Multiclamp 700B amplifier (Molecular Devices) and a Digidata 1550A data acquisition system (Molecular Devices). Dissected larvae were incubated in HL-3 containing 0.375 mM (for mEJP) or 2 mM (for EJP and PPR) Ca^{2+}, and a recording electrode filled with 3 M KCl was inserted into muscle 6 of the A3 or A4 segment containing NMJs. All data were analyzed using Mini-Analysis software (Synaptosoft). PPR was calculated as a ratio of EJP amplitudes with paired stimulation (50 msec interval). QC was calculated as the average EJP amplitude divided by the average mEJP amplitude as previously described (Lee et al., 2010).

2.8. VMAT-pHluorin Live Imaging

VMAT-pHluorin live imaging was previously described (Shiba-Fukushima et al., 2014). Briefly, the DA release rates of neuronal fibers and terminals in the whole brain region without the subesophageal ganglion were calculated by normalizing the data with the fluorescence intensity just after photobleaching using ImageJ software.

2.9. Statistical Analysis

Error bars in graphs represent the mean ± SEM. A two-tailed Student's *t*-test or a one-way repeated-measures analysis of variance (ANOVA) was used to determine significant differences between two or among multiple groups, respectively, unless otherwise indicated. If a significant result was determined using ANOVA ($p < 0.05$), the mean values of the control and the specific test group were analyzed using a Tukey-Kramer test. Steel's test and Dunnett's test were used to determine significant differences between two specific groups or among multiple groups of interest. The data distribution was assumed to be normal, although this assumption was not formally tested. Randomization was used in each genotype, and data collection and analysis were not performed blind to the conditions of the experiments. All the data obtained in the experiments were included except for the VMAT-pHluorin assay, for which the samples that showed increased fluorescence signals immediately after photobleaching were excluded.

3. Results

3.1. Removal of One Copy of TBPH Improves the Decreased Motor Ability and Lifespan Caused by PS Mutation

The amino acid residues of p150^{Glued} affected in PS are highly conserved between humans and *Drosophila* (Farrer et al., 2009; Lloyd et al., 2012). To understand how PS-associated mutations of p150^{Glued} affect neurons, we expressed wild-type p150^{Glued} (p150^{WT}) and a mutant, p150^{Glued}, in which Gly50 is replaced with Arg (p150^{G50R}; corresponding to p150^{G71R} in humans) in *Drosophila* dopaminergic neurons. Forty-five-day-old normal adult flies exhibited an age-dependent decline in compulsive motor activity compared with 5-day-old flies; this decline was exacerbated in flies expressing p150^{G50R} (Fig. 1A). The introduction of a *TAR DNA-binding protein of 43 homolog* (*TBPH*) null allele, *TBPH*$^{\Delta 23}$, caused an approximately 30% reduction in TBPH protein levels (Fig. S1A, B) (Feiguin et al., 2009; Diaper et al., 2013b) and improved motor disturbances caused by p150^{WT} or p150^{G50R} (Fig. 1A, lower). Whereas the lifespan of *TBPH*$^{+/-}$ flies was reduced compared to controls, the combination of *TBPH*$^{+/-}$ with p150^{WT} or p150^{G50R} improved

Fig. 2. Motor neuron-specific p150^{G50R} expression produces swelling of terminal boutons at NMJs. (A) Distal (d) and four proximal boutons (p) of NMJs. Arrowheads indicate synaptic debris visualized with anti-HRP. Scale bar, 5 μm. (B, C) Size (B) and number (C) of synapse boutons. $n = 16$–23 NMJ terminals (B) or 8–10 NMJs (C) in 5 flies per genotype, $^{*}p < 0.05$ *vs.* Control by Steel's test. The sample size is indicated in the graphs. (D) Active zones (AZs, red) at the synaptic boutons stained with anti-HRP (Blue). Scale bar, 2 μm. (E) Average number of AZs per bouton from distal and four proximal boutons. $n = 20$–39 NMJ terminals in 5 flies per genotype, $^{*}p < 0.05$ *vs.* Control by Dunnett's test. The sample size is indicated in the graph. (F) DCVs (green) at the synaptic boutons stained with anti-HRP (red). Scale bar, 5 μm. (G) Graphs for DCV aggregates with over 0.5 μm^2 in the most distal boutons (left) and average DCV density in the most distal boutons and in the proximal three boutons (right). A.U., arbitrary units. $n = 10$–13 NMJ terminals in 6 flies per genotype, $^{*}p < 0.05$ by two-tailed Student's *t*-test. $^{\#}p < 0.05$ *vs.* Control; TBPH$^{+/+}$, $^{\S}p < 0.05$ *vs.* Control; TBPH$^{+/-}$ by Dunnett's test. The sample size is indicated in the graphs. See also Fig. S2. Genotypes used: (A–E) *OK6-Gal4/+* (Control), *OK6-Gal4/UAS-p150^{G50R}-HA* (p150^{G50R}), *OK6-Gal4, TBPH$^{\Delta 23}$/+* (TBPH$^{+/-}$), *OK6-Gal4, TBPH$^{\Delta 23}$/UAS-p150^{G50R}-HA* (p150^{G50R}; TBPH$^{+/-}$), (F, G) *UAS-preproANF-EMD/+*; *+/+*; *D42-Gal4/+* (Control), *UAS-preproANF-EMD/+*; *UAS-p150^{WT}-HA/+*; *D42-Gal4/+* (p150^{WT}), *UAS-preproANF-EMD/+*; *UAS-p150^{G50R}-HA/+*; *D42-Gal4/+* (p150^{G50R}), *UAS-preproANF-EMD/+*; *TBPH$^{\Delta 23}$/+*; *D42-Gal4/+* (TBPH$^{+/-}$), *UAS-preproANF-EMD/+*; *TBPH$^{\Delta 23}$/UAS-p150^{WT}-HA*; *D42-Gal4/+* (p150^{WT}; TBPH$^{+/-}$), *UAS-preproANF-EMD/+*; *TBPH$^{\Delta 23}$/UAS-p150^{G50R}-HA*; *D42-Gal4/+* (p150^{G50R}; TBPH$^{+/-}$).

the lifespan of $p150^{WT}$ or $p150^{G50R}$ flies (Fig. 1B). We did not observe decreased spontaneous locomotor activity, loss of TH-positive neurons or decreased total amount of brain dopamine in flies expressing $p150^{WT}$ or $p150^{G50R}$ even in 45-day-old flies (Fig. S1C–E). However, the removal of a copy of *TBPH* stimulated spontaneous locomotor activity (Fig. S1C).

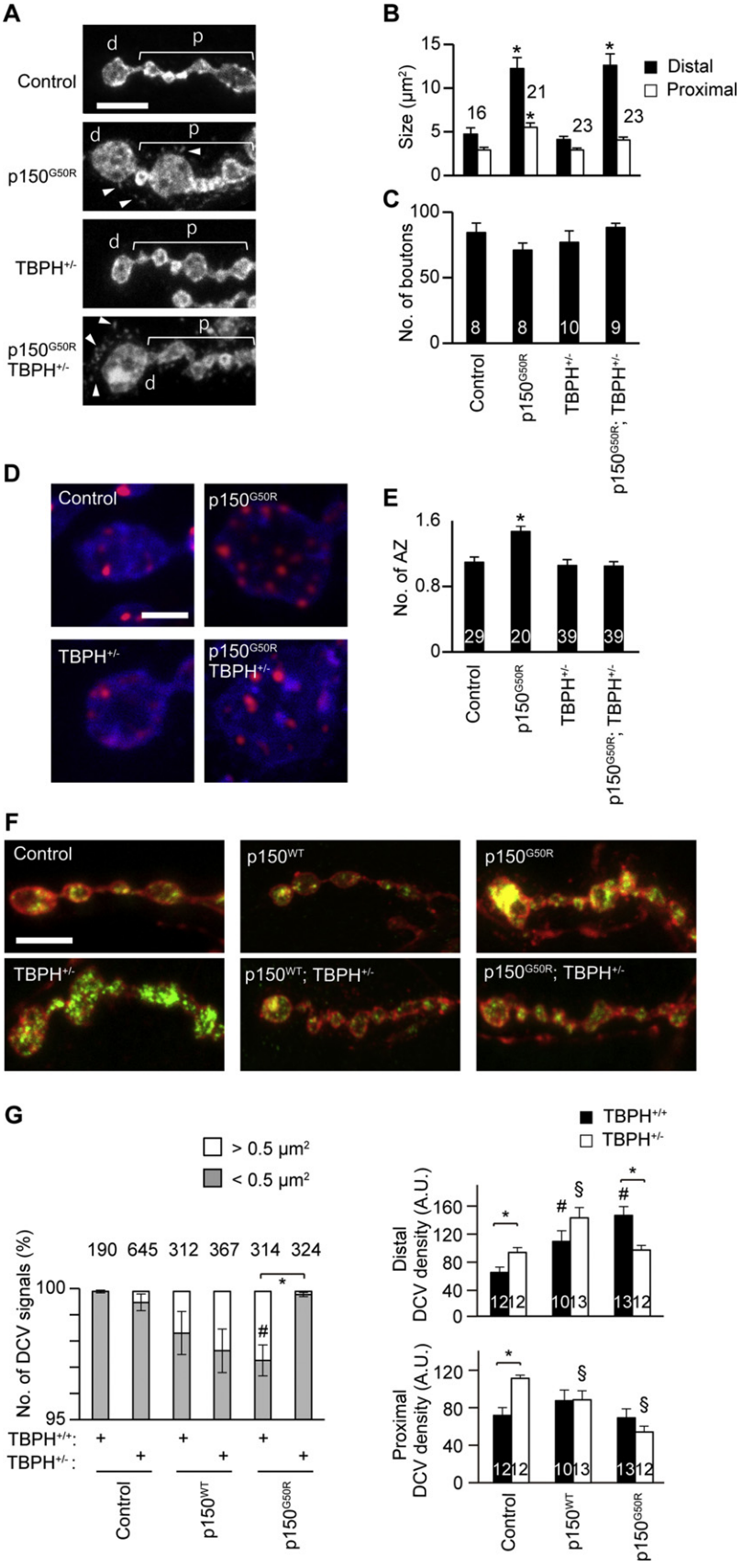

3.2. Axonal Terminals are Affected by PS Mutation

Previous studies have suggested that $p150^{Glued}$ is required for synapse growth and stabilization (Eaton et al., 2002; Chang et al., 2013). These events appear to be regulated by $p150^{Glued}$-mediated stabilization of microtubule plus ends and to be abrogated in the Perry mutant G74P (Lazarus et al., 2013). The expression of $p150^{G50R}$ in larval motor neurons caused both distal and proximal synaptic boutons to swell with prominent synaptic debris (Fig. 2A, B) (Fuentes-Medel et al., 2009), but the number of synaptic boutons was not significantly changed (Fig. 2C), thus suggesting that the G50R mutation has moderate effects on $p150^{Glued}$ function. The swollen synaptic phenotype of proximal but not distal boutons by $p150^{G50R}$ was suppressed in the $TBPH^{+/-}$ background, whereas the synaptic phenotypes of $TBPH^{+/-}$ were similar to those of controls (Fig. 2A–C). In this context, $TBPH^{+/-}$ did not suppress the synaptic debris observed in $p150^{G50R}$ synapses (Fig. 2A). The number of AZs in $p150^{G50R}$ synapses increased, possibly as a consequence of an alteration to the signaling pathway for AZ development, accompanied by endocytic defects (Dickman et al., 2006). This phenotype was suppressed by the introduction of $TBPH^{+/-}$ (Fig. 2D, E). Alteration of presynaptic structures may affect the maturation and maintenance of the postsynaptic architecture (Romano et al., 2014). We therefore examined the distribution and expression of a postsynaptic scaffold protein, Dlg, and a subunit of the postsynaptic glutamate receptor, GluRIIA, in the neuromuscular junctions (NMJs) of larval motor neurons (Fig. S1A and S2A). Whereas Dlg expression appeared to be unchanged, GluRIIA tended to be reduced by $p150^{G50R}$ expression or removal of a copy of *TBPH*, thus suggesting that postsynaptic functions are partially affected.

Because mitochondrial dysfunction is thought to be part of the etiology of Parkinson's disease, we also analyzed mitochondrial distribution in NMJs (Fig. S2B) (Imai and Lu, 2011). Unexpectedly, smaller mitochondria accumulated in the most distal boutons in $TBPH^{+/-}$ larvae. The mitochondrial number of the terminal 6 boutons, especially the proximal 5 boutons, of the NMJs in $p150^{G50R}$ and $p150^{G50R}$ $TBPH^{+/-}$ larvae tended to be lower, whereas the mitochondrial density in the most distal boutons was not significantly changed among genotypes. These observations suggest that TBPH reduction did not reverse the altered mitochondrial distribution caused by $p150^{G50R}$.

A decrease in dopamine release is an early event of dopaminergic neurodegeneration in PS as well as Parkinson's disease (Wider and Wszolek, 2008), and monoamine neurotransmitters are thought to be stored in both dense core vesicles (DCVs) and synaptic vesicles in *Drosophila* (Grygoruk et al., 2014). A uniform supply of DCVs in each bouton is achieved by a circulation of axonal flow and a local capture mechanism. To visualize the distribution of DCVs in the NMJs, emerald GFP-tagged atrial natriuretic factor (ANF-EMD) was expressed in motor neurons (Fig. 2F and Fig. S2C) (Rao et al., 2001). Most DCVs were approximately 0.5 μm^2 in dimension in control animals, whereas the expression of $p150^{G50R}$ resulted in the accumulation of aggregated DCVs over 0.5 μm^2 in the most distal boutons (Left graph in Fig. 2G and Fig. S2C). In contrast, the density of DCVs was increased in proximal boutons of $TBPH^{+/-}$ larvae (Right graph in Fig. 2G). Importantly, the accumulation of DCVs in the most distal boutons by $p150^{G50R}$ was suppressed, and the uniform distribution of DCVs was observed at a level similar to controls *via* the *TBPH* reduction (Fig. 2F, G and Fig. S2C). Although the expression of $p150^{WT}$ mildly promoted DCV aggregation in the most distal boutons, the phenotype was not changed by decreased *TBPH*, thus suggesting that the beneficial effect on the bouton DCV dynamics by decreased *TBPH* is $p150^{G50R}$ specific (Fig. 2F, G and Fig. S2C).

3.3. TBPH Contributes to Defects in Axonal Transport of DCVs

We next monitored the movement of DCVs in the axonal transport of larval motor neurons (Fig. 3A and Movies S1, S2, S3, S4). Larger DCVs tended to appear in $TBPH^{+/-}$ animals (Fig. 3A, B and Fig. S3A). The expression of $p150^{WT}$ caused moderate DCV aggregates, which were suppressed by the removal of a copy of *TBPH* (Fig. 3A, B and Fig. S3A). The $p150^{G50R}$ expression resulted in the marked appearance of large DCV aggregates, which were also alleviated by the decreased *TBPH* (Fig. 3A, B and Fig. S3A). In sharp contrast, the morphology of axonal mitochondria was mostly unchanged by the expression of $p150^{G50R}$, and mitochondria were not colocalized with TBPH, even with an ALS-associated mutant (Fig. S3B, C) (Wang et al., 2016). Whereas $p150^{WT}$ affected the retrograde transport of DCVs, which caused increased stationary DCVs, $p150^{G50R}$ markedly impaired DCV movement in both anterograde and retrograde directions and further increased stationary DCVs (Fig. 3C–E and Fig. S3D, E). In addition, the number of retrograde DCVs that reversed to an anterograde flow was significantly increased after expression of $p150^{G50R}$ but not $p150^{WT}$, thus suggesting that retrograde transport is especially compromised by $p150^{G50R}$ (Fig. 3C, F and Fig. S3F). The introduction of $TBPH^{+/-}$ partially rescued these defects *via* $p150^{WT}$ or $p150^{G50R}$ (Fig. 3C–F and Fig. S3D, E), whereas the reduction in the velocity of DCVs by $p150^{G50R}$ was not improved (Fig. 3G). Consistently with defects in the axonal transport of DCVs, the decreased dopamine release estimated by VMAT-pHluorin in the adult brain of $p150^{G50R}$ flies was also alleviated by the introduction of $TBPH^{+/-}$ (Fig. 3H and Fig. S3G). However, we did not detect a physical interaction of TBPH with $p150^{Glued}$ (Fig. S3H) or decreased endogenous $p150^{Glued}$ and dynein after introducing $TBPH^{+/-}$ (Fig. S1A, B). These results suggest that the rescue effects of $p150^{G50R}$ phenotypes associated with decreased TBPH levels are an indirect mechanism.

3.4. Dysfunction of Synaptic Release by the PS Mutation Is Rescued by TBPH Reduction

Given that synaptic activity is impaired by the blockage of DCV transport in $p150^{G50R}$-expressing neurons, we next analyzed the electrophysiological properties of the NMJ in larval motor neurons. The excitatory junction potential (EJP) and quantal content (QC) were reduced

Fig. 3. $p150^{G50R}$ leads to a disturbance of axonal flow and aggregation of DCVs in motor neurons. (A) DCVs in motor neuron axons. Scale bars, 200 (upper) and 5 (lower) μm. (B) Size distribution of DCVs. The number of DCVs larger than 0.5 μm^2 is increased in $p150^{WT}$ and $p150^{G50R}$. $n = 148$–1317 DCVs from 5 to 10 axons in 4–5 larvae per genotype, $^{*}p < 0.05$ *vs.* Control; $TBPH^{+/+}$ by Dunnett's test, $^{\#}p < 0.05$ by two-tailed Student's *t*-test. Removal of a copy of TBPH partially suppresses the appearance of large DVCs in $p150^{WT}$ and $p150^{G50R}$ (lower). (C) Disturbance of axonal DCV movement is partially rescued by TBPH reduction. Representative kymographs generated from axonal movies. The x-axis represents DCV position, and the y-axis is time (moving from top to bottom). Vertical lines correspond to stationary DCVs, and diagonal lines are moving DCVs. The bottom panels reveal the track of only the moving DCVs, which are shown as blue (anterograde) or red (retrograde) diagonal lines. (D–F) The percentage of moving DCVs (D) and of stationary DCVs (E). $n = 148$ DCVs from 9 larvae (control), 282 DCVs from 12 larvae ($TBPH^{+/-}$), 176 DCVs from 12 larvae ($p150^{G50R}$), and 344 DCVs from 15 larvae ($p150^{G50R}$; $TBPH^{+/-}$), $^{*}p < 0.05$, $^{**}p < 0.01$ by Tukey-Kramer test. The percentage of DCVs that reverse the direction from anterograde (A) to retrograde (R) flow or in the opposite direction during movement (F). $^{*}p < 0.05$ by two-tailed Student's *t*-test. (G) The average velocity of DCVs. $n = 148$ DCVs from 9 larvae (control), 282 DCVs from 12 larvae ($TBPH^{+/-}$), 176 DCVs from 12 larvae ($p150^{G50R}$), and 344 DCVs from 15 larvae ($p150^{G50R}$; $TBPH^{+/-}$), $^{**}p < 0.01$ by Tukey-Kramer test. (H) Recovery ratio of VMAT-pHluorin in a 30-day-old adult brain. $n = 6$–10 per genotype, $^{*}p < 0.05$ *vs.* Control by Dunnett's test. The sample size is indicated in parentheses. See also Fig. S3 and Movies S1, S2, S3, S4. Genotypes used: (A–G) *UAS-preproANF-EMD/+*; *+/+*; *D42-Gal4/+* (Control), *UAS-preproANF-EMD/+*; $TBPH^{\Delta 23}$*/+*; *D42-Gal4/+* ($TBPH^{+/-}$), *UAS-preproANF-EMD/+*; *UAS-*$p150^{WT}$*-HA/+*; *D42-Gal4/+* ($p150^{WT}$), *UAS-preproANF-EMD/+*; *UAS-*$p150^{G50R}$*-HA/+*; *D42-Gal4/+* ($p150^{G50R}$), *UAS-preproANF-EMD/+*; $TBPH^{\Delta 23}$*/UAS-*$p150^{WT}$*-HA*; *D42-Gal4/+* ($p150^{WT}$; $TBPH^{+/-}$), *UAS-preproANF-EMD/+*; $TBPH^{\Delta 23}$*/UAS-*$p150^{G50R}$*-HA*; *D42-Gal4/+* ($p150^{G50R}$; $TBPH^{+/-}$), (H) *+/Y*; *+/+*; *TH-Gal4*, *UAS-VMAT-pHluorin/+* (Control), *+/Y*; *UAS-*$p150^{G50R}$*-HA/+*; *TH-Gal4*, *UAS-VMAT-pHluorin/+* ($p150^{G50R}$), *+/Y*; $TBPH^{\Delta 23}$*/+*; *TH-Gal4*, *UAS-VMAT-pHluorin/+* ($TBPH^{+/-}$), *+/Y*; *UAS-*$p150^{G50R}$*-HA/*$TBPH^{\Delta 23}$; *TH-Gal4*, *UAS-VMAT-pHluorin/+* ($p150^{G50R}$; $TBPH^{+/-}$).

in p150^{G50R} but not p150^{WT} animals, thus suggesting impaired synaptic release in PS (Fig. 4A). Consistently with results from morphological analyses of synaptic boutons, *TBPH* reduction improved the EJP and QC of p150^{G50R} animals. However, the miniature excitatory junction potential (mEJP) frequency was increased in p150^{WT} animals, thus suggesting that p150^{WT} overexpression partially affects synaptic activity (Fig. 4A, B

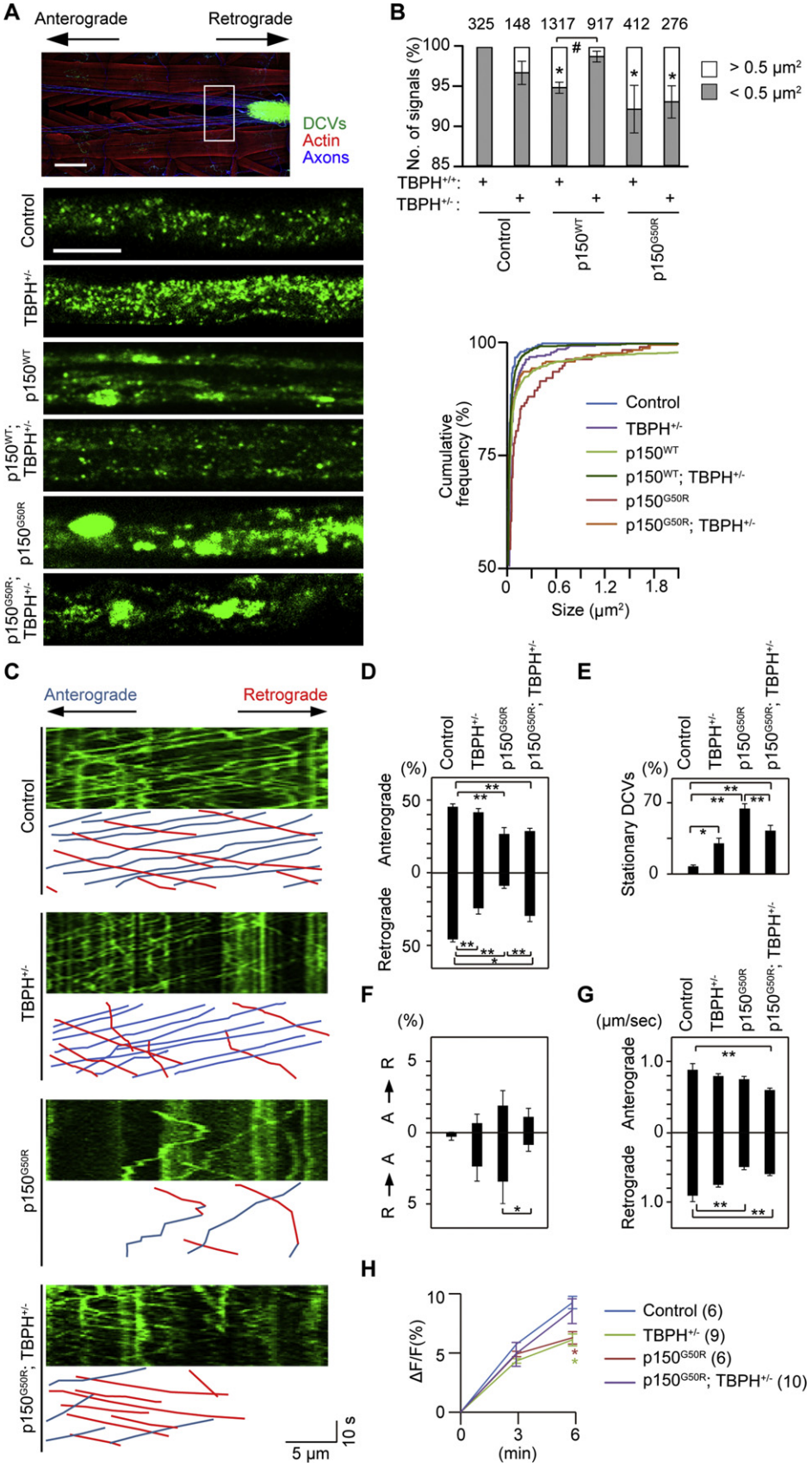

and Table S1). The $p150^{WT}$ and $TBPH^{+/-}$ animals tended to exhibit larger spikes in mEJPs, and the large spikes of $TBPH^{+/-}$ animals were suppressed by $p150^{G50R}$ expression (Fig. 4B, C). The paired-pulse ratio (PPR) was not different among the five genotypes (Table S1).

Consistently with the increased mEJP frequency, the number of synaptic vesicles (SVs) was increased in both the AZ regions and the presynaptic cytosol of $TBPH^{+/-}$ NMJs, thus suggesting that TBPH at synapses is important for the regulation of SVs (Fig. 4D, E and Fig. S4). The enlarged boutons of $p150^{G50R}$-expressing neurons contained fewer SVs docked at AZs, but many DCVs and uncharacterized large vesicular structures with high or low electron density, which probably include aggregated DCVs and lysosomes (Fig. 4D and Fig. S4B) (Lloyd et al., 2012). Again, the appearance of abnormal vesicular structures was suppressed by the decreased TBPH in $p150^{G50R}$-expressing neurons (Fig. 4D).

4. Discussion

Whereas mutations of $p150^{Glued}$ cause PS, in which TDP-43 pathology has been reported in the basal ganglia, including the substantia nigra, whether TDP-43 contributes to neurodegeneration in PS remained unknown. Here, we analyzed the molecular relationship between $p150^{Glued}$ and TDP-43 in a *Drosophila* PS model.

Neuronal expression of the $p150^{G50R}$ mutation, located in the CAP-Gly domain, led to swelling of distal boutons and the prominent aggregation of DCVs but not mitochondria in axons and synapses. DCVs travel between proximal axons and terminal boutons *via* axonal transport, which efficiently delivers neurotransmitters to synaptic boutons (Wong et al., 2012). Although $p150^{G50R}$ disrupts both the anterograde and retrograde flow of DCVs, the anterograde/retrograde ratios of moving DCVs suggested that the retrograde flow is especially affected by $p150^{G50R}$ (Fig. 3D), thus leading to accumulation of organelles and materials at nerve terminals (Fig. 4D). Consistently with the morphological abnormalities in synaptic phenotypes, synaptic strength, dopamine release and motor ability were decreased by $p150^{G50R}$ expression without detectable neuron loss. Although $p150^{WT}$ expression also affected the retrograde flow of DCVs and the DCV distribution at the terminal boutons, the phenotypes were milder than those of $p150^{G50R}$. Given that $p150^{WT}$ protein was expressed at higher levels than $p150^{G50R}$ in our transgenic flies, in which both $p150^{WT}$ and $p150^{G50R}$ transgenes were inserted in the same genomic locus and both transcript levels were similar, $p150^{G50R}$ exerts highly deleterious effects on neuronal activity despite its unstable expression (Lloyd et al., 2012). Thus, our data obtained with $p150^{G50R}$ expression would reflect synaptic dysfunction as an early neurodegeneration event in PS.

Altered mitochondrial distribution at the boutons by $p150^{G50R}$ was not significantly rescued by TBPH reduction, thus suggesting that the improvement of DCV phenotypes markedly contributes to the rescue effects in neuronal functions and survival. However, we cannot exclude the possibility that mitochondrial functions may be affected in $p150^{G50R}$ flies, because the fluorescence intensity of mitoGFP (cytochrome C oxidase subunit VIII-GFP fusion protein), which inserts in the mitochondrial inner membrane in a membrane potential-dependent manner, was somewhat reduced by $p150^{G50R}$. Ultrastructural analysis of synaptic mitochondria also suggested that mitochondrial cristae were partly damaged in $p150^{G50R}$ flies (Fig. 4D). Because mitochondrial shuttling between cell bodies and nerve terminals in neurons would be important to maintain mitochondrial proteins derived from the nuclear genome, which include the respiratory complex I, III, IV and V subunits, the effects of PS mutations on mitochondrial functions at nerve terminals should be examined in future studies (Abe et al., 1995).

TDP-43 accumulation in affected regions is a prominent feature of PS pathology. TDP-43 forms cytoplasmic messenger ribonucleoprotein (mRNP) granules, which also move *via* axonal transport to synaptic boutons to deliver mRNA for synaptic activities (Alami et al., 2014). Our discovery in *Drosophila* that the ablation of a copy of the *TBPH* gene improves the axonal aggregation of DCVs and synaptic defects provides three possible molecular mechanisms: First, a reduced concentration of TBPH in axons and nerve terminals improves axonal flow, suppressing the aggregation of TBPH. Second, TBPH reduction alters the expression of proteins regulated by TBPH at transcript levels, thus alleviating synaptic dysfunctions. Third, the above two mechanisms contribute to rescue effects. We prefer the third mechanism for the reasons listed below.

The DCV aggregates in axons and synapses were suppressed by TBPH reduction without improving the velocity of axonal transport, thus suggesting that aggregation-prone TBPH promotes DCV aggregation when the axonal flow stagnates. However, the numbers of DCVs and SVs were increased in the synaptic boutons of $TBPH^{+/-}$ flies, thus suggesting that TBPH negatively regulates DCV and SV production. A variety of TBPH target mRNAs have been reported in *Drosophila* (Hazelett et al., 2012; Vanden Broeck et al., 2013; Coyne et al., 2014), and further studies may reveal a target(s) to regulate DCVs and SVs. Regarding synaptic stabilization, microtubule-associated MAP1B/Futsch is an evolutionarily conserved target of TDP-43/TBPH, which negatively or positively regulates synaptic MAP1B/Futsch expression (Sephton et al., 2010; Godena et al., 2011; Coyne et al., 2014) and might maintain axonal transport through regulating microtubule dynamics. Although we did not detect obvious changes in the levels of Futsch protein in $TBPH^{+/-}$ flies (data not shown), the downregulation of Futsch/MAP1B may explain the observation that some phenotypes in $TBPH^{+/-}$ flies were reversed by $p150^{G50R}$ expression. Because $p150^{Glued}$ stabilizes the plus ends of microtubules, the ectopic expression of $p150^{G50R}$ may partially alleviate the microtubule destabilization caused by Futsch/MAP1B downregulation (Lazarus et al., 2013). Alternatively, the decreased axonal flow resulting from $p150^{G50R}$ expression may enable efficient synaptic capture of TDP-43-mRNP granules, which regulate local protein translation for synaptic activity including Futsch/MAP1B (Diaper et al., 2013b; Alami et al., 2014).

Autoregulation of TDP-43 mRNA has been demonstrated in mammals (Ayala et al., 2011; Polymenidou et al., 2011) and has been suggested in *Drosophila* (Hazelett et al., 2012; Vanden Broeck et al., 2013). Consistently with these reports, the decrease in TBPH protein was at most 30% in $TBPH^{+/-}$ flies. Although the genetic ablation of a copy of the *TBPH* gene in itself produced some synaptic phenotypes and decreased the lifespan in flies, the transient knockdown of TDP-43 would be a suitable strategy for therapeutic intervention in PS. It has been demonstrated that the transient inhibition of a truncated N-terminal huntingtin with an abnormal polyQ stretch improves the neuropathology and the motor phenotype in a Huntington's disease mouse model (Yamamoto et al., 2000). Thus, disease phenotypes caused by

Fig. 4. Reduced TBPH rescues synaptic strength at the NMJs of $p150^{G50R}$ flies. (A) Representative electrophysiological traces of EJP and mEJP in the larval NMJs. Scale bar for EJP (mEJP): y = 10 mV (3 mV), x = 50 msec (1 s). EJP amplitudes (EJP) and quantal content (QC) are reduced in $p150^{G50R}$ flies. $^{*(\#)}p < 0.05$ *vs.* Control by Steel's test (Dunnett's test). Black dots indicate large spikes (>1.5 mV) in mEJP. See also Table S1 for further electrophysiological information. (B, C) Cumulative spike numbers (B) and number of large spikes (C) during 60 s. $n = 4–10$ NMJs in 4–6 flies per genotype. The number of large spikes in (C) was not significantly altered among the genotypes, on the basis of Dunnett's test. The sample size is indicated in the graph of (C). (D) Ultrastructural images of the synapse boutons in the larval motor neurons. M, mitochondria. Arrowheads, large DCVs. Abnormal vesicular structures in $p150^{G50R}$ flies are also indicated by asterisks. Scale bar, 500 nm. (E) Quantification of the SV number in the unit area containing an AZ (defined in Fig. S4A). $n = 8–23$ AZ neighboring regions in 3 flies, $^{*}p < 0.05$ *vs.* Control by Dunnett's test. The sample size is indicated in the graph. See also Table S1 and Fig. S4. Genotypes used: *OK6-Gal4*, *UAS-mitoGFP*/+ (Control), *OK6-Gal4*, *UAS-mitoGFP*/*UAS-$p150^{WT}$-HA* ($p150^{WT}$), *OK6-Gal4*, *UAS-mitoGFP*/*UAS-$p150^{G50R}$-HA* ($p150^{G50R}$), *OK6-Gal4*, *UAS-mitoGFP*, $TBPH^{\Delta 23}$/+ ($TBPH^{+/-}$), *OK6-Gal4*, *UAS-mitoGFP*, $TBPH^{\Delta 23}$/*UAS-$p150^{G50R}$-HA* ($p150^{G50R}$; $TBPH^{+/-}$).

TDP-43 proteinopathies may be reversible under appropriate levels of TDP-43 control.

Supplementary data to this article can be found online at http://dx.doi.org/10.1016/j.ebiom.2017.06.002.

Funding Sources

This study was funded by Grants-in-Aid for Scientific Research (26293070 [Y.I.], 15H04842 [N.H.]) from MEXT in Japan, a Grant-in-

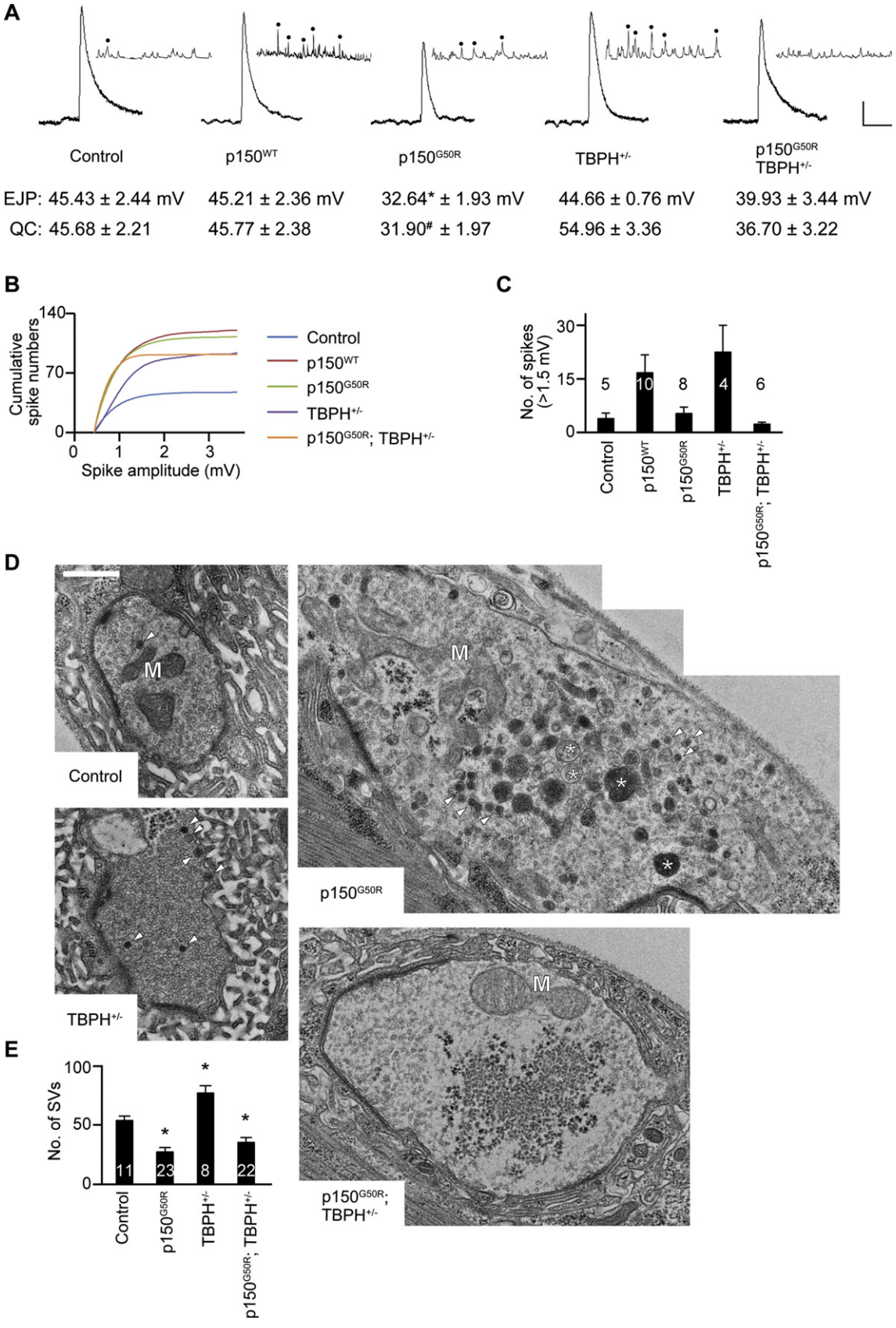

Aid for Scientific Research on Innovative Areas (23111003 [N.H.]), a Health Labor Sciences Research Grant (201324123A) (N.H. and Y.I.), and a grant from Otsuka Pharmaceutical (N.H. and Y.I.).

Conflicts of Interest

The authors have no conflicts of interest to declare.

Author Contributions

Y.I. conceived and designed the study. Y.H. and T.I. performed most of the experiments and analyzed the data with support from K.S., C.C., and T.A. Y.H., Y.I., and N.H. wrote the manuscript with input from the other authors.

Acknowledgments

We thank Drs. F. Feiguin, F.E. Baralle, T.E. Lloyd, A.L. Kolodkin, D.C. Zarnescu, V.I. Gelfand, C.Q. Doe, F. Hirth, T. Chihara and M. Miura for providing materials, and we thank T. Imura, T. Kanao, Y. Umezaki, M. Yoshida and S. Kakuta for their technical assistance.

References

Abe, K., Aoki, M., Kawagoe, J., Yoshida, T., Hattori, A., Kogure, K., Itoyama, Y., 1995. Ischemic delayed neuronal death. A mitochondrial hypothesis. Stroke 26, 1478–1489.

Alami, N.H., Smith, R.B., Carrasco, M.A., Williams, L.A., Winborn, C.S., Han, S.S., Kiskinis, E., Winborn, B., Freibaum, B.D., Kanagaraj, A., Clare, A.J., Badders, N.M., Bilican, B., Chaum, E., Chandran, S., Shaw, C.E., Eggan, K.C., Maniatis, T., Taylor, J.P., 2014. Axonal transport of TDP-43 mRNA granules is impaired by ALS-causing mutations. Neuron 81, 536–543.

Arai, T., Hasegawa, M., Akiyama, H., Ikeda, K., Nonaka, T., Mori, H., Mann, D., Tsuchiya, K., Yoshida, M., Hashizume, Y., Oda, T., 2006. TDP-43 is a component of ubiquitin-positive tau-negative inclusions in frontotemporal lobar degeneration and amyotrophic lateral sclerosis. Biochem. Biophys. Res. Commun. 351, 602–611.

Ayala, Y.M., De Conti, L., Avendano-Vazquez, S.E., Dhir, A., Romano, M., D'Ambrogio, A., Tollervey, J., Ule, J., Baralle, M., Buratti, E., Baralle, F.E., 2011. TDP-43 regulates its mRNA levels through a negative feedback loop. EMBO J. 30, 277–288.

Ayloo, S., Lazarus, J.E., Dodda, A., Tokito, M., Ostap, E.M., Holzbaur, E.L., 2014. Dynactin functions as both a dynamic tether and brake during dynein-driven motility. Nat. Commun. 5, 4807.

Chang, L., Kreko, T., Davison, H., Cusmano, T., Wu, Y., Rothenfluh, A., Eaton, B.A., 2013. Normal dynactin complex function during synapse growth in *Drosophila* requires membrane binding by Arfaptin. Mol. Biol. Cell 24 (1749–1764), S1741–S1745.

Chiang, P.M., Ling, J., Jeong, Y.H., Price, D.L., Aja, S.M., Wong, P.C., 2010. Deletion of TDP-43 down-regulates Tbc1d1, a gene linked to obesity, and alters body fat metabolism. Proc. Natl. Acad. Sci. U. S. A. 107, 16320–16324.

Coyne, A.N., Siddegowda, B.B., Estes, P.S., Johannesmeyer, J., Kovalik, T., Daniel, S.G., Pearson, A., Bowser, R., Zarnescu, D.C., 2014. Futsch/MAP1B mRNA is a translational target of TDP-43 and is neuroprotective in a *Drosophila* model of amyotrophic lateral sclerosis. J. Neurosci. 34, 15962–15974.

Diaper, D.C., Adachi, Y., Lazarou, L., Greenstein, M., Simoes, F.A., Di Domenico, A., Solomon, D.A., Lowe, S., Alsubaie, R., Cheng, D., Buckley, S., Humphrey, D.M., Shaw, C.E., Hirth, F., 2013a. *Drosophila* TDP-43 dysfunction in glia and muscle cells cause cytological and behavioural phenotypes that characterize ALS and FTLD. Hum. Mol. Genet. 22, 3883–3893.

Diaper, D.C., Adachi, Y., Sutcliffe, B., Humphrey, D.M., Elliott, C.J., Stepto, A., Ludlow, Z.N., Vanden Broeck, L., Callaerts, P., Dermaut, B., Al-Chalabi, A., Shaw, C.E., Robinson, I.M., Hirth, F., 2013b. Loss and gain of *Drosophila* TDP-43 impair synaptic efficacy and motor control leading to age-related neurodegeneration by loss-of-function phenotypes. Hum. Mol. Genet. 22, 1539–1557.

Dickman, D.K., Lu, Z., Meinertzhagen, I.A., Schwarz, T.L., 2006. Altered synaptic development and active zone spacing in endocytosis mutants. Curr. Biol. 16, 591–598.

Eaton, B.A., Fetter, R.D., Davis, G.W., 2002. Dynactin is necessary for synapse stabilization. Neuron 34, 729–741.

Estes, P.S., Boehringer, A., Zwick, R., Tang, J.E., Grigsby, B., Zarnescu, D.C., 2011. Wild-type and A315T mutant TDP-43 exert differential neurotoxicity in a *Drosophila* model of ALS. Hum. Mol. Genet. 20, 2308–2321.

Farrer, M.J., Hulihan, M.M., Kachergus, J.M., Dachsel, J.C., Stoessl, A.J., Grantier, L.L., Calne, S., Calne, D.B., Lechevalier, B., Chapon, F., Tsuboi, Y., Yamada, T., Gutmann, L., Elibol, B., Bhatia, K.P., Wider, C., Vilarino-Guell, C., Ross, O.A., Brown, L.A., Castanedes-Casey, M., Dickson, D.W., Wszolek, Z.K., 2009. DCTN1 mutations in Perry syndrome. Nat. Genet. 41, 163–165.

Feiguin, F., Godena, V.K., Romano, G., D'Ambrogio, A., Klima, R., Baralle, F.E., 2009. Depletion of TDP-43 affects *Drosophila* motoneurons terminal synapsis and locomotive behavior. FEBS Lett. 583, 1586–1592.

Fiesel, F.C., Voigt, A., Weber, S.S., Van den Haute, C., Waldenmaier, A., Gorner, K., Walter, M., Anderson, M.L., Kern, J.V., Rasse, T.M., Schmidt, T., Springer, W., Kirchner, R., Bonin, M., Neumann, M., Baekelandt, V., Alunni-Fabbroni, M., Schulz, J.B., Kahle, P.J., 2010. Knockdown of transactive response DNA-binding protein (TDP-43) downregulates histone deacetylase 6. EMBO J. 29, 209–221.

Fuentes-Medel, Y., Logan, M.A., Ashley, J., Ataman, B., Budnik, V., Freeman, M.R., 2009. Glia and muscle sculpt neuromuscular arbors by engulfing destabilized synaptic boutons and shed presynaptic debris. PLoS Biol. 7, e1000184.

Godena, V.K., Romano, G., Romano, M., Appocher, C., Klima, R., Buratti, E., Baralle, F.E., Feiguin, F., 2011. TDP-43 regulates *Drosophila* neuromuscular junctions growth by modulating Futsch/MAP1B levels and synaptic microtubules organization. PLoS One 6, e17808.

Grygoruk, A., Chen, A., Martin, C.A., Lawal, H.O., Fei, H., Gutierrez, G., Biedermann, T., Najibi, R., Hadi, R., Chouhan, A.K., Murphy, N.P., Schweizer, F.E., Macleod, G.T., Maidment, N.T., Krantz, D.E., 2014. The redistribution of *Drosophila* vesicular monoamine transporter mutants from synaptic vesicles to large dense-core vesicles impairs amine-dependent behaviors. J. Neurosci. 34, 6924–6937.

Hazelett, D.J., Chang, J.C., Lakeland, D.L., Morton, D.B., 2012. Comparison of parallel high-throughput RNA sequencing between knockout of TDP-43 and its overexpression reveals primarily nonreciprocal and nonoverlapping gene expression changes in the central nervous system of *Drosophila*. G3 (Bethesda) 2, 789–802.

Imai, Y., Lu, B., 2011. Mitochondrial dynamics and mitophagy in Parkinson's disease: disordered cellular power plant becomes a big deal in a major movement disorder. Curr. Opin. Neurobiol. 21, 935–941.

Josephs, K.A., Whitwell, J.L., Tosakulwong, N., Weigand, S.D., Murray, M.E., Liesinger, A.M., Petrucelli, L., Senjem, M.L., Ivnik, R.J., Parisi, J.E., Petersen, R.C., Dickson, D.W., 2015. TAR DNA-binding protein 43 and pathological subtype of Alzheimer's disease impact clinical features. Ann. Neurol. 78, 697–709.

Lazarus, J.E., Moughamian, A.J., Tokito, M.K., Holzbaur, E.L., 2013. Dynactin subunit p150(glued) is a neuron-specific anti-catastrophe factor. PLoS Biol. 11, e1001611.

Lee, S., Liu, H.P., Lin, W.Y., Guo, H., Lu, B., 2010. LRRK2 kinase regulates synaptic morphology through distinct substrates at the presynaptic and postsynaptic compartments of the *Drosophila* neuromuscular junction. J. Neurosci. 30, 16959–16969.

Li, Y., Ray, P., Rao, E.J., Shi, C., Guo, W., Chen, X., Woodruff 3rd, E.A., Fushimi, K., Wu, J.Y., 2010. A *Drosophila* model for TDP-43 proteinopathy. Proc. Natl. Acad. Sci. U. S. A. 107, 3169–3174.

Ling, J.P., Pletnikova, O., Troncoso, J.C., Wong, P.C., 2015. TDP-43 repression of nonconserved cryptic exons is compromised in ALS-FTD. Science 349, 650–655.

Lloyd, T.E., Machamer, J., O'Hara, K., Kim, J.H., Collins, S.E., Wong, M.Y., Sahin, B., Imlach, W., Yang, Y., Levitan, E.S., McCabe, B.D., Kolodkin, A.L., 2012. The p150(glued) CAP-Gly domain regulates initiation of retrograde transport at synaptic termini. Neuron 74, 344–360.

McAleese, K.E., Walker, L., Erskine, D., Thomas, A.J., McKeith, I.G., Attems, J., 2017. TDP-43 pathology in Alzheimer's disease, dementia with Lewy bodies and ageing. Brain Pathol. 27, 472–479.

Moughamian, A.J., Holzbaur, E.L., 2012. Dynactin is required for transport initiation from the distal axon. Neuron 74, 331–343.

Neumann, M., Sampathu, D.M., Kwong, L.K., Truax, A.C., Micsenyi, M.C., Chou, T.T., Bruce, J., Schuck, T., Grossman, M., Clark, C.M., McCluskey, L.F., Miller, B.L., Masliah, E., Mackenzie, I.R., Feldman, H., Feiden, W., Kretzschmar, H.A., Trojanowski, J.Q., Lee, V.M., 2006. Ubiquitinated TDP-43 in frontotemporal lobar degeneration and amyotrophic lateral sclerosis. Science 314, 130–133.

Nonaka, T., Masuda-Suzukake, M., Arai, T., Hasegawa, Y., Akatsu, H., Obi, T., Yoshida, M., Murayama, S., Mann, D.M., Akiyama, H., Hasegawa, M., 2013. Prion-like properties of pathological TDP-43 aggregates from diseased brains. Cell Rep. 4, 124–134.

Perry, T.L., Bratty, P.J., Hansen, S., Kennedy, J., Urquhart, N., Dolman, C.L., 1975. Hereditary mental depression and Parkinsonism with taurine deficiency. Arch. Neurol. 32, 108–113.

Polymenidou, M., Lagier-Tourenne, C., Hutt, K.R., Huelga, S.C., Moran, J., Liang, T.Y., Ling, S.C., Sun, E., Wancewicz, E., Mazur, C., Kordasiewicz, H., Sedaghat, Y., Donohue, J.P., Shiue, L., Bennett, C.F., Yeo, G.W., Cleveland, D.W., 2011. Long pre-mRNA depletion and RNA missplicing contribute to neuronal vulnerability from loss of TDP-43. Nat. Neurosci. 14, 459–468.

Puls, I., Jonnakuty, C., LaMonte, B.H., Holzbaur, E.L., Tokito, M., Mann, E., Floeter, M.K., Bidus, K., Drayna, D., Oh, S.J., Brown Jr., R.H., Ludlow, C.L., Fischbeck, K.H., 2003. Mutant dynactin in motor neuron disease. Nat. Genet. 33, 455–456.

Rao, S., Lang, C., Levitan, E.S., Deitcher, D.L., 2001. Visualization of neuropeptide expression, transport, and exocytosis in *Drosophila melanogaster*. J. Neurobiol. 49, 159–172.

Romano, G., Klima, R., Buratti, E., Verstreken, P., Baralle, F.E., Feiguin, F., 2014. Chronological requirements of TDP-43 function in synaptic organization and locomotive control. Neurobiol. Dis. 71, 95–109.

Sephton, C.F., Good, S.K., Atkin, S., Dewey, C.M., Mayer 3rd, P., Herz, J., Yu, G., 2010. TDP-43 is a developmentally regulated protein essential for early embryonic development. J. Biol. Chem. 285, 6826–6834.

Shiba-Fukushima, K., Inoshita, T., Hattori, N., Imai, Y., 2014. PINK1-mediated phosphorylation of Parkin boosts Parkin activity in *Drosophila*. PLoS Genet. 10, e1004391.

Siller, K.H., Serr, M., Steward, R., Hays, T.S., Doe, C.Q., 2005. Live imaging of *Drosophila* brain neuroblasts reveals a role for Lis1/dynactin in spindle assembly and mitotic checkpoint control. Mol. Biol. Cell 16, 5127–5140.

Swarup, V., Phaneuf, D., Bareil, C., Robertson, J., Rouleau, G.A., Kriz, J., Julien, J.P., 2011. Pathological hallmarks of amyotrophic lateral sclerosis/frontotemporal lobar degeneration in transgenic mice produced with TDP-43 genomic fragments. Brain 134, 2610–2626.

Tacik, P., Fiesel, F.C., Fujioka, S., Ross, O.A., Pretelt, F., Castaneda Cardona, C., Kidd, A., Hlavac, M., Raizis, A., Okun, M.S., Traynor, S., Strongosky, A.J., Springer, W., Wszolek, Z.K., 2014. Three families with Perry syndrome from distinct parts of the world. Parkinsonism Relat. Disord. 20, 884–888.

Tan, R.H., Kril, J.J., Fatima, M., McGeachie, A., McCann, H., Shepherd, C., Forrest, S.L., Affleck, A., Kwok, J.B., Hodges, J.R., Kiernan, M.C., Halliday, G.M., 2015. TDP-43 proteinopathies: pathological identification of brain regions differentiating clinical phenotypes. Brain 138, 3110–3122.

Vanden Broeck, L., Naval-Sanchez, M., Adachi, Y., Diaper, D., Dourlen, P., Chapuis, J., Kleinberger, G., Gistelinck, M., Van Broeckhoven, C., Lambert, J.C., Hirth, F., Aerts, S., Callaerts, P., Dermaut, B., 2013. TDP-43 loss-of-function causes neuronal loss due to defective steroid receptor-mediated gene program switching in *Drosophila*. Cell Rep. 3, 160–172.

Volkening, K., Leystra-Lantz, C., Yang, W., Jaffee, H., Strong, M.J., 2009. Tar DNA binding protein of 43 kDa (TDP-43), 14-3-3 proteins and copper/zinc superoxide dismutase (SOD1) interact to modulate NFL mRNA stability. Implications for altered RNA processing in amyotrophic lateral sclerosis (ALS). Brain Res. 1305, 168–182.

Wang, W., Wang, L., Lu, J., Siedlak, S.L., Fujioka, H., Liang, J., Jiang, S., Ma, X., Jiang, Z., da Rocha, E.L., Sheng, M., Choi, H., Lerou, P.H., Li, H., Wang, X., 2016. The inhibition of TDP-43 mitochondrial localization blocks its neuronal toxicity. Nat. Med. 22, 869–878.

Wider, C., Wszolek, Z.K., 2008. Rapidly progressive familial parkinsonism with central hypoventilation, depression and weight loss (Perry syndrome)–a literature review. Parkinsonism Relat. Disord. 14, 1–7.

Wider, C., Dickson, D.W., Stoessl, A.J., Tsuboi, Y., Chapon, F., Gutmann, L., Lechevalier, B., Calne, D.B., Personett, D.A., Hulihan, M., Kachergus, J., Rademakers, R., Baker, M.C., Grantier, L.L., Sujith, O.K., Brown, L., Calne, S., Farrer, M.J., Wszolek, Z.K., 2009. Pallidonigral TDP-43 pathology in Perry syndrome. Parkinsonism Relat. Disord. 15, 281–286.

Wong, M.Y., Zhou, C., Shakiryanova, D., Lloyd, T.E., Deitcher, D.L., Levitan, E.S., 2012. Neuropeptide delivery to synapses by long-range vesicle circulation and sporadic capture. Cell 148, 1029–1038.

Wu, T.H., Lu, Y.N., Chuang, C.L., Wu, C.L., Chiang, A.S., Krantz, D.E., Chang, H.Y., 2013. Loss of vesicular dopamine release precedes tauopathy in degenerative dopaminergic neurons in a *Drosophila* model expressing human tau. Acta Neuropathol. 125, 711–725.

Yamamoto, A., Lucas, J.J., Hen, R., 2000. Reversal of neuropathology and motor dysfunction in a conditional model of Huntington's disease. Cell 101, 57–66.